Angular distribution in two-photon double ionization of helium by intense attosecond soft-x-ray pulses

Imre F. Barna,[1,2] Jianyi Wang,[1,3] and Joachim Burgdörfer[1]
[1]*Institute for Theoretical Physics, Vienna University of Technology, A1040 Vienna Austria, European Union*
[2]*Radiation and Environmental Physics Department, KFKI Atomic Energy Research Institute, P.O. Box 49, H-1525 Budapest, Hungary, European Union*
[3]*Department of Physics, University of Massachusetts Dartmouth, North Dartmouth, Massachusetts 02747, USA*
(Received 16 November 2005; published 2 February 2006)

We investigate two-photon double ionization of helium by intense ($\approx 10^{15}$ W/cm^2) ultrashort ($\approx$300 as) soft-x-ray pulses (E=91.6 eV). The time-dependent two-electron Schrödinger equation is solved using a coupled channel method. We show that for ultrashort pulses the angular distribution of ejected electrons depends on the pulse duration and provides insight into the role of electron correlations in the two-electron photoemission process. The angular distribution at energies near the "independent-electron" peaks is close to dipolar while it acquires in the "valley" of correlated emission a significant quadrupolar component within a few hundred attoseconds.

DOI: 10.1103/PhysRevA.73.023402 PACS number(s): 32.80.Rm, 32.80.Fb

I. INTRODUCTION

Recent advances in the high-order harmonic generation (HHG) techniques have led to the development of soft-x-ray sources that feature ultrashort pulses with pulse durations of a few hundred attoseconds (as) [1] and may reach intensities ($\gtrsim 10^{14}$ W/cm^2) that are capable of inducing multiphoton processes. Extreme ultraviolet (xuv) pulses (photon energy 27.9 eV) with pulse duration of 950 as have been characterized with an autocorrelation technique [2]. Recently, the two-photon double ionization and above-threshold ionization of helium were experimentally observed with the Ti:sapphire 27th harmonic pulses (photon energy 41.8 eV) [3]. These experimental advances open up the opportunity to revisit the dynamics of double ionization of helium by xuv photons previously investigated only in the single-photon absorption and scattering regime using synchrotron radiation [4,5]. Simultaneous ejection of two electrons by a single photon allowed detailed tests of wave functions for the three-body Coulomb problem [6–8] and the role of electron correlations in strongly inelastic processes accompanied with near-zero momentum transfer (photoabsorption) or sizable momentum transfer (Compton scattering) [9,10].

Multiphoton, in particular two-photon, ionization of helium by xuv pulses has been studied theoretically by different groups. A considerable numerical effort has been made to solve the two-active electron time-dependent Schrödinger equation (TDSE) with various methods. The *R*-matrix Floquet theory was successful to describe the $(2\gamma, 2e)$ process of He [11] in the photon energy range between where absorption of two photons are necessary for double ionization. The configuration interaction *B*-spline spectral method [12,13] was applied to solve the TDSE for this problem. The products of two *B* splines represent the radial part of the wave function which allows the inclusion of the electron-electron interaction to a high degree of accuracy. Colgan *et al.* [14] developed a time-dependent coupled channel method and studied the complete fragmentation of helium at 45 eV photon energy and presented fully differential cross sections. Recently Lambropoulos *et al.* [15] found a "knee" structure in the intensity dependence reminiscent of a similar knee shape for double ionization by strong IR pulses [16]. Photons above the double ionization threshold ($\omega_{\mathrm{xuv}} > 2.9$ a.u. or 79 eV) were considered by Parker *et al.* [17] who performed the direct numerical integration of the two-electron TDSE with a mixed finite-difference–basis set approach on a lattice and studied double ionization with 87 eV photon energy pulses with a laser peak intensity around 10^{16} W/cm^2. They analyzed both sequential as well as nonsequential double ionization events by a varying number of absorbed photons for long pulses ($\tau_p \gtrsim 2$ fs). Most recently, Ishikawa and Midorikawa [18] investigated two-photon double ionization by ultrashort pulses with durations of $\tau_p \approx 150$–450 as pertinent to HHG sources. They identified an "anomalous" component in the electron spectrum in between the two peaks associated with sequential double ionization and discussed its possible origin in terms of post-ionization energy exchange and core relaxation effects.

In this paper, we theoretically investigate two-photon double ionization of helium by ultrashort attosecond pulses as a function of time by solving the TDSE with our coupled channel method which has been originally developed for heavy-ion helium collisions [19–21] and later implemented to describe laser-driven atomic processes and two-photon coherent control [22]. We consider experimentally realized high-intensity laser pulses with 13.5 nm wavelength [23] which are the 59th harmonic of a Ti:sapphire laser (wavelength 800 nm). The photon energy considered (91.6 eV) is larger than the double ionization threshold of He (79 eV). A single photon is thus sufficient to induce double ionization. This case has been studied in detail with weak-field synchrotron sources where multiphoton effects are absent. Because one photon can interact with one electron only, double ionization cannot occur without electron-electron interaction. The picture is that one electron is directly ionized by absorbing the photon, and the second electron leaves through electron correlation either in the initial or in the final state, or both. This has been discussed in terms of a shake-off and

electron-electron scattering (often referred to as TS1 [24]).

In contrast, for intense fields considered here, there is sufficient photon flux such that two photons can be absorbed, one by each electron, and the pair of electrons is ejected. Electron correlation is therefore not a prerequisite for double ionization to occur. At the same time, the ponderomotive energy of the xuv pulse $E_P=8\pi I/4c\omega_{\rm xuv}^2$ is so small that ionization by the rescattering of the first ionized and accelerated electron that causes "nonsequential" double ionization by strong IR pulses [25,26] can be ruled out. We discuss the conceptual difficulties in applying notions of sequential and nonsequential double ionization to such short pulses. We show that the angular distribution provides detailed insights into the ionization process on the attosecond time scale. The role electron correlation plays in this process can be identified.

II. SCENARIO FOR TWO-PHOTON DOUBLE IONIZATION BY ATTOSECOND xuv PULSES: TIME SEQUENCE AND CORRELATION

We consider a linearly polarized attosecond xuv pulse with a Gaussian envelope

$$F(t) = F_0 \exp\left[-2\ln 2\frac{t^2}{\tau_p^2}\right]\cos(\omega_{\rm xuv}t)\mathbf{e}_z, \tag{1}$$

where τ_p is the full width at half maximum (FWHM) of the pulse intensity. The center frequency $\omega_{\rm xuv}$ corresponds to a Ti:sapphire 59th harmonic pulse with the energy of 91.6 eV. Following Ref. [18] we will consider pulse durations $\tau_p=150$ and 450 as corresponding to $\tau_p=6.25$ and $\tau_p=18.7$ a.u. The period of the xuv cycle is $T=2\pi/\omega_{\rm xuv}\cong 1.9$ a.u. The xuv pulse [Eq. (1)] subtends only few cycles (3 to 10) and therefore closely resembles few-cycle optical or near-IR pulses. The significant Fourier broadening therefore precludes the appearance of spectrally sharp photoionization peaks. There is, however, a fundamental difference to optical pulses of the same intensity: even at an intensity of $I=10^{15}$ W/cm^2, the quiver amplitude of a free electron $\sqrt{8\pi I/c}/\omega_{\rm xuv}^2\approx 0.01$ a.u. is small on an atomic scale. Likewise, the ponderomotive energy $E_P=8\pi I/4c\omega_{\rm xuv}^2\approx 0.006$ a.u. is negligibly small. Therefore, ionization takes place deep in the (multi) photon regime rather than in the tunnel ionization regime applicable to IR pulses of the same intensity. This difference has immediate consequences for the notion of "(non) sequential" ionization. While for tunnel ionization the time window Δt of an individual ionization "burst" can be uniquely identified near the field maxima with subcycle precision [27], the multiphoton ionization event is intrinsically delocalized in time over several cycles. Only then does the electron response to an electromagnetic pulse mimic that of photon absorption. In view of the fact that the entire xuv pulse duration τ_p subtends only a few cycles, it is obvious that the notion of sequentiality of ionization events loses its meaning in the present case. This is in sharp contrast to intense field ionization by optical fields. There, the first ionization by tunnel ionization under the influence of a quasiclassical electric field is well localized and separated in time from the collisional ionization of the second electron upon rescattering. The observed scaling with the pulse duration $\propto\tau_p^N$, where N is the number of photons absorbed, should therefore not be taken as evidence of (non) sequentiality but a measure of the total energy absorbed from the radiation field during τ_p. The uncertainty in time when the absorption process takes place or, equivalently, time delocalization of the multiphoton processes does not imply that all time-differential information on the ionization process is averaged out, as will be shown below.

The time characterizing the pulse duration should be compared to the time scale of the electronic motion. Using the approximate hydrogenic expression for the classical orbital period

$$\tau_0 = 2\pi n^3/Z_{\rm eff}^2, \tag{2}$$

the orbital period ranges between $\tau_0=40$ as (=1.6 a.u.) for the "inner" electron of $He^+(1s)(Z_{\rm eff}=2)$ and, for the "outer" electron of He $(1s^2)$ with a binding energy of 24.6 eV ($Z_{\rm eff}=1.3$), $\tau_0=90$ as ($\approx$4 a.u.) The cycle period T and the orbital period are comparable to each other, thus probing the electronic motion on the time scale on which the two interacting electrons of the helium ground-state exchange energy, linear, and angular momentum. Thus, double ionization by attosecond xuv pulses may probe electron correlations in both initial and final states.

The role of correlation in double photoionization of helium is a well-established subject in the low-intensity or single-photon limit of xuv radiation going back to the pioneering paper by Byron and Joachain [28]. As the electron-photon interaction is a one-body operator, single-photon absorption can directly eject only one electron. Ejecting a second electron requires with necessity electron-electron interaction. The latter does not, however, inevitably imply correlation effects. Adhering here and in the following to the identification of correlation with those pieces of the interaction not included in a mean-field or independent particle (IP) model as embodied in the (single configuration) Hartree-Fock description [24], one-photon double ionization can proceed via mean-field contribution. Already the sudden change of the screening following the ejection of the first electron generates a finite probability of ejecting a second electron. This "shake-off" process accounts for about 40% of the total doble ionization cross sections at high photon energies. Clearly, for a quantitatively accurate description, in particular over the entire range of photon energies from threshold to high energies [8] correlation effects beyond the mean field in both the initial and final states are essential.

For two-photon double ionization by xuv pulses with $\omega_{\rm xuv}>2$ a.u. dominance of independent-particle (IP) ionization is expected since each reaction

$$\mathrm{He} + \hbar\omega_{\rm xuv} \rightarrow \mathrm{He}^+(nl) + e^-, \tag{3}$$

$$\mathrm{He}^+(nl) + \hbar\omega_{\rm xuv} \rightarrow \mathrm{He}^{++} + e^-, \tag{4}$$

where n and l are the principal and angular momentum quantum numbers of He^+, respectively, is energetically allowed for all n. The quantum numbers, $n=1$ and $l=0$ are expected to dominate in Eqs. (3) and (4). Thus, correlation effects

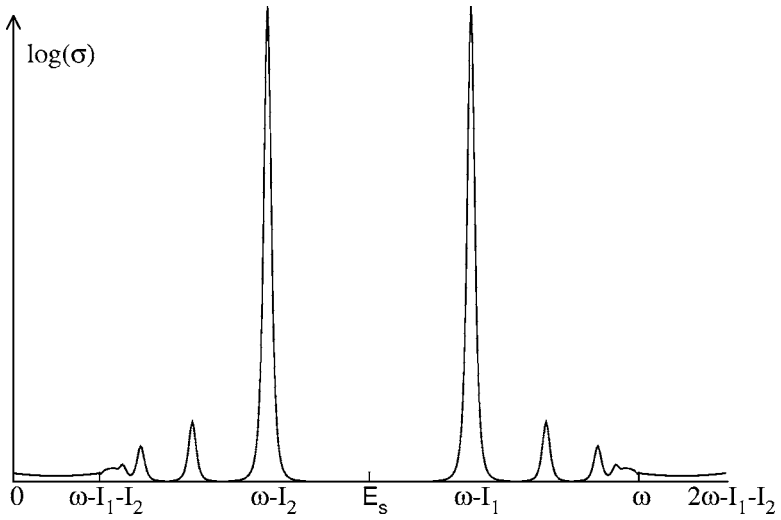

FIG. 1. Electron spectrum following two-photon absorption ($\omega \equiv \omega_{\mathrm{xuv}} = 91.6$ eV) in coincidence with He^{2+}, schematically. The symmetric energy sharing corresponds to $E_S = \omega_{\mathrm{xuv}} - (I_1 + I_2)/2$ with $I_{1,2}$ being the first and second ionization potentials, respectively.

appear to be unimportant for the two-photon process. It should be noted that the picture of a chain of reactions each satisfying energy conservation in the photoelectric effect separately, invoked by Eqs. (3) and (4), is only meaningful for $\tau_p \to \infty$. In this limit, Eqs. (3) and (4), implies an electron spectrum in coincidence with He^{++} (displayed schematically in Fig. 1) with two Rydberg series symmetrically centered around the energy

$$E_S = \omega_{\mathrm{xuv}} - (I_1 + I_2)/2 = 52 \text{ eV}. \tag{5}$$

The single-photon double ionization spectrum well known from synchrotron studies appears as a continuum below 12.6 eV ($\omega_{\mathrm{xuv}} - I_1 - I_2$). Its two-photon replica would set in above $E = \omega_{\mathrm{xuv}} = 91.6$ eV. For ultrashort τ_p all discrete peaks get dramatically broadened and merge into a quasi-continuum.

Apart from the broadening, the limit of short τ_p has further consequences when this time becomes comparable to the electronic correlation time τ_C in the helium ground state. The latter can be simply estimated from the characteristic time for exchange of energy and angular momentum between two classical electrons. Alternatively, it can be estimated from the correlation energy $E_C = E - E_{\mathrm{HF}}$ as $\tau_C = 1/E_C$. In either cases, τ_C is of the order 10 a.u. (or 200 as). xuv pulses with periods T of 2 a.u. and durations of 3–10 a.u. therefore can probe the correlation dynamics.

It is instructive to visualize the two-photon double ionization process diagrammatically (Fig. 2). The two photon lines each representing the one-body operator of photoabsorption end either at the same or at two different electrons resulting in two different diagrams. (The line representing the nucleus has been omitted for simplicity.) It should be noted that a definite time ordering of the vertices of electron-photon interactions is neither implied nor meaningful for ultrashort pulses in light of the discussion above. The dashed lines refer to electron-electron interaction in the initial and final states which lead to energy and angular momentum exchange. The latter is reflected in a configuration-interaction wave function in terms of admixtures of orbitals of different single-particle angular momenta

$$|\Psi_i\rangle = \sum_{i,j} a_s^{(i,j)} |s^i\rangle |s^j\rangle + \sum_{i,j} a_p^{(i,j)} |p^i\rangle |p^j\rangle + \sum_{i,j} a_d^{(i,j)} |d^i\rangle |d^j\rangle + \cdots . \tag{6}$$

Typical orders of magnitude of admixture coefficients for the initial state are [28] [see also Eq. (15) below] $|a_p/a_s| \lesssim 0.1$, $|a_d/a_s| \lesssim 0.01$ and those of higher l are exceedingly small. The admixture of non-s orbitals to the He ground state provides a unique signature of electron correlation as it would be absent in an IP or HF model. More precisely, $l \neq 0$ configurations represent angular correlation while coefficients $a_s^{(i,j)}$ may contain radial correlation. Correspondingly, angular momentum components in the final state reflect both the angular momentum transfer $\Delta l = \pm 1$ by photoabsorption as well as the non-s admixtures due to electron correlations in the initial and final state. Their presence can be mapped out by the time dependence of the angular distribution of ejected electrons.

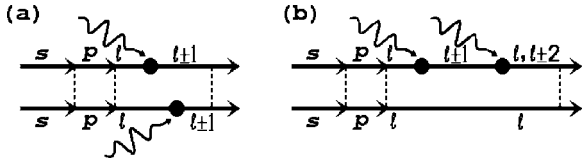

FIG. 2. Schematic interaction diagrams for two-photon absorption from He ground state. (a) Each electron absorbs one photon each; (b) one electron absorbs two photons. Dashed lines denote the electron-electron interactions.

III. COMPUTATIONAL METHOD

We have calculated the double ionization by two-photon absorption represented by the diagrams of Fig. 2 using our time-dependent coupled-channel method. The point to be noted is that while we discuss and interpret our results within to lowest-order perturbation theory (LOPT), the calculation is fully nonperturbative taking into account electron-photon and electron-electron interactions to all orders, albeit within a truncated basis. Briefly, we calculate ionization process of the helium atom in the laser pulse by solving the TDSE equation

$$i\frac{\partial}{\partial t}\Psi(\mathbf{r}_1,\mathbf{r}_2,t) = [\hat{H}_{\mathrm{He}} + \hat{V}(t)]\Psi(\mathbf{r}_1,\mathbf{r}_2,t), \tag{7}$$

for the atomic Hamiltonian

$$\hat{H}_{\mathrm{He}} = \frac{\mathbf{p}_1^2}{2} + \frac{\mathbf{p}_2^2}{2} - \frac{2}{r_1} - \frac{2}{r_2} + \frac{1}{|\mathbf{r}_1 - \mathbf{r}_2|}, \tag{8}$$

and with the laser-electron interaction

$$\hat{V}(t) = -\sum_{i=1,2} \mathbf{F}(t)\cdot\mathbf{r}_i, \tag{9}$$

in the length gauge and the dipole approximation. The laser pulses are linearly polarized along the z axis with the time dependence given by Eq. (1). We expand $\Psi(\mathbf{r}_1,\mathbf{r}_2,t)$ in the basis $\{\Phi_j\}$ of eigenfunctions of the time-independent Schrödinger equation

$$\hat{H}\Phi_j(\mathbf{r}_1,\mathbf{r}_2) = E_j\Phi_j(\mathbf{r}_1,\mathbf{r}_2) \tag{10}$$

to yield

$$\Psi(\mathbf{r}_1,\mathbf{r}_2,t) = \sum_{j=1}^{N} c_j(t)\Phi_j(\mathbf{r}_1,\mathbf{r}_2)e^{-iE_jt}, \tag{11}$$

where the $a_j(t)$ are the time-dependent expansion coefficients and E_j are the eigenvalues of Eq. (10). Inserting Eq. (11) into the TDSE (7) leads to the system of first-order differential equations for the expansion coefficients

$$\frac{dc_k(t)}{dt} = -i\sum_{j=1}^{N} V_{kj}e^{i(E_k-E_j)t}c_j(t) \quad (k=1,\ldots,N). \tag{12}$$

Denoting the ground state by $k=1$, we impose the initial condition

$$c_k(t\to-\infty) = \begin{cases} 1, & k=1, \\ 0, & k\neq 1. \end{cases} \tag{13}$$

The asymptotic probabilities for transitions into final states k after the pulse has been turned off are given by

$$P_k = |c_k(t\to+\infty)|^2. \tag{14}$$

The ionization probability can be retrieved from P_k which includes discretized channels representing the continuum formed by the wave packets. The equations of coupled channels (12) are solved by a Runge-Kutta-Fehlberg integrator of order five with automatic time step adjustment.

The eigenfunctions Φ_j in Eq. (10) are obtained by diagonalizing the Hamiltonian in a basis of orthogonal symmetrized two-particle functions f_μ

$$\Phi_j(\mathbf{r}_1,\mathbf{r}_2) = \sum_\mu b_\mu^{[j]} f_\mu(\mathbf{r}_1,\mathbf{r}_2). \tag{15}$$

In the following we restrict ourselves to singlet helium states. The two-particle functions are made up of symmetrized single particle orbitals $g_{\epsilon l}(r)Y_l^m$, where the radial functions $g_{\epsilon l}$ consist of radial Slater functions and radial regular Coulomb wave packets. We note that the coefficients $b_\mu^{[j]}$ are related to the admixture coefficients discussed earlier following Eq. (6). The wave packets form a discrete representation of the Coulomb continuum and can serve as building blocks of our finite basis [19,20].

We include single-particle wave functions with $0\leqslant l_1, l_2 \leqslant 2$ angular momenta and couple them to $0\leqslant L\leqslant 2$ total angular momentum two-electron states. For the $L=0$ configurations we use $ss+pp+dd$ angular correlated wave functions, for $L=1$ we use $sp+pd$ couplings and for $L=2$ the $sd+pp+dd$ configurations, respectively. Since already the contribution of d orbitals in the present case is found to be small, higher l_i can be safely neglected. The angular correlated contributions play an essential role to understanding the angular distribution of the ionized electrons. In order to determine the final electronic state population, the expectation value of the reduced one-electron density operator $\hat{\rho}=\Sigma_{i=1,2}\delta(\mathbf{r}-\mathbf{r}_i)$ is calculated after the laser pulse

$$\rho(\vec{r}) = \langle\Psi(t\to\infty)|\hat{\rho}|\Psi(t+\infty)\rangle. \tag{16}$$

We employ the Feshbach projection method [20] to separate the singly ionized states from the doubly ionized states. Accordingly, the one-electron polar angular distribution of ionized electrons in the double ionization channel is given by

$$\begin{aligned} P_{\mathrm{DI}}(\theta) &= \frac{1}{2\pi}\int_0^{2\pi}\int_0^{\infty}\langle\Psi_{\mathrm{DI}}|\sum_{i=1,2}\delta(\mathbf{r}-\mathbf{r}_i)|\Psi_{\mathrm{DI}}\rangle r^2 dr d\varphi \\ &= \frac{1}{\pi}\int_0^{2\pi}\int_0^{\infty}\int_{\mathbf{r}_1}|\Psi_{\mathrm{DI}}(r,\theta,\varphi;\mathbf{r}_1)|^2 d\mathbf{r}_1 r^2 dr d\varphi, \end{aligned} \tag{17}$$

where Ψ_{DI} represents the projection of Ψ onto the subspace of doubly ionized states.

IV. RESULTS AND DISCUSSION

Before analyzing the angular distribution from Eq. (17) we briefly present results for the energy distribution for which a direct comparison with a recent calculation by Ishikawa and Midorikawa [18] is possible. The single electron energy distribution integrated over the second electron for the pulse duration of 450 as (Fig. 3) features two prominent peaks which can be easily identified with help of Fig. 1 as the ionization spectra following the reactions (3) and (4). The dominant yet strongly broadened peak at 67 eV (labeled c) is due to electrons ejected from the ground state of He with the first ionization potential of $I_1=24.6$ eV. In the second interaction, the electrons are ejected from the He^+ ion with an ionization potential of $I_2=54.4$ eV, yielding the peak at $91.6-I_2=37.2$ eV (labeled a). From the higher members or the Rydberg series only $n=2$ peaks are identifiable in Fig. 3 as local humps, one just below and one above the main peaks, respectively. Structures from $n\geqslant 3$ are not visible since their contributions become exceedingly small. The cross section of the single-photon double ionization continuum below 12.6 eV (see Fig. 1) is by far too small to be visible on a linear scale. The peaks a and c (Fig. 3) have been previously referred to as sequential ionization [18] or above-threshold ionization [17]. We will refer to this process as independent particle (IP) ionization to stress that electron

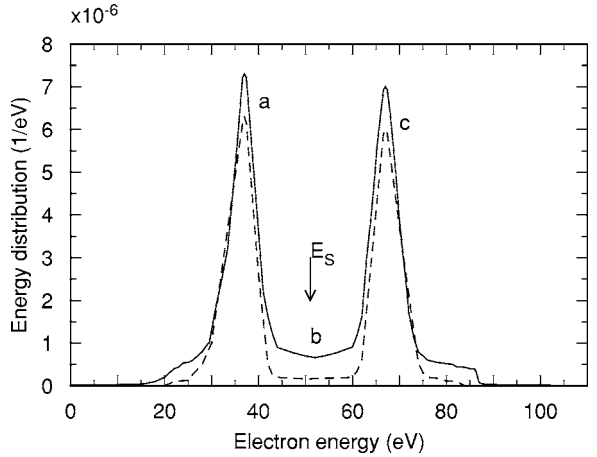

FIG. 3. Energy distribution of the ejected electrons in two-photon double ionization of He. The peak intensity of the pulse is 10^{15} W/cm^2 and the pulse duration is τ_p=450 as. The solid line represents our results and the dashed line represents the data for Ishikawa *et al.* [18]. The energy positions referred to in text are 37.2 eV (a), 52 eV (b), and 67 eV (c).

correlation effects play no significant role in their occurrence. This is in striking contrast to the spectral feature in the "valley" (labeled *b*) (also referred to as anomalous component [18]) in which correlation effects are of crucial importance. We refer to this feature as "correlation induced" (CI) ionization.

The dependence of the CI ionization on the pulse duration τ_p is illustrated in Fig. 4 for an ultrashort pulse of 150 as. The valley is now quite shallow and a significant fraction of the ionization probability is contained in the "valley." This is, in the first place, an obvious consequence of the increased Fourier broadening in the ultrashort pulse limit. In the opposite limit $\tau_p \gg T$ and $\tau_p \gg \tau_0$, the spectrum is expected to revert to the quasidiscrete line spectrum, schematically depicted in Fig. 1. Only in the long-pulse limit, the notions of time ordering or sequentiality of the process takes on physical meaning. Overall, our data agree with those of Ref. [18] remarkably well on an absolute scale with the largest discrepancies in the wings of the peak for the 10 cycle pulse (450 as).

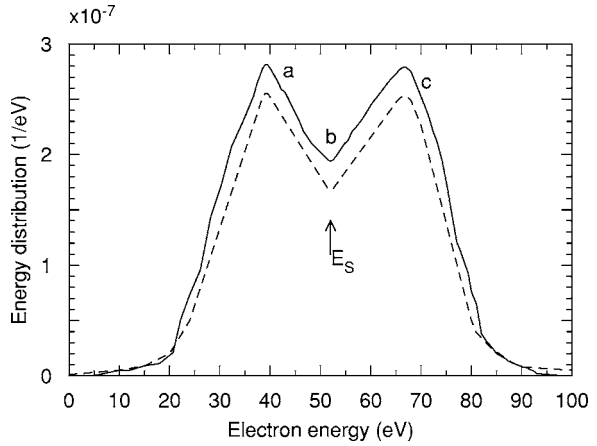

FIG. 4. Notation is the same as in Fig. 3, but for τ_p=150 as. The marked energy positions are 39 eV (a), 52 eV (b), and 67 eV (c).

The identification of the valley region near E_s with correlated ionization is, in the first instance, taken over from one-photon double ionization by synchrotron radiation where the region of symmetric energy sharing of the available photon energy is dominated by correlation effects [24]. The extension of this identification to two-photon absorption can be quantitatively justified by the properties of the angular distribution, as shown below. Were the valley simply the result of the Fourier broadening of two IP peaks, the distribution $P_{\mathrm{DI}}(\theta)$ at the energies near (E_S) should closely resemble those of the spectral regions (a) or (c). That this is not at all the case is illustrated by the polar plot (Fig. 5) of the angular distribution near the IP ionization peak (a) and the CI ionization valley (b). The different contour line indicates the time evolution of the angular distribution in increments of 50 as for the 450 as pulse. While the IP peak retains the emission pattern of a Hertz dipole during the entire pulse duration, the CI electron distribution takes on a pronounced nondipolar, i.e., quadrupolar, pattern after about 150 as. The onset of a nondipolar distribution on this time scale can be also observed for the ultrashort pulse of τ_p=150 as (Fig. 6) indicating that the sharp differences in the angular distribution between the IP peak and the CI component is also present when the valley is very shallow. For the ultrashort pulse a slight peak shift from 37 to about 39 eV is found in agreement with Ref. [18].

The anisotropy of the angular distribution can be characterized by the multipole expansion

$$\frac{d\sigma}{d\Omega} = \frac{\sigma_0}{4\pi}[1 + \beta P_2(\cos\theta) + \gamma P_4(\cos\theta)], \tag{18}$$

where σ_0 is the integral cross section, $P_{2,4}$ are the Legendre polynomials, and β and γ are the second-order $(k=2)$ and fourth-order $(k=4)$ anisotropy parameters, respectively. Note that a "dipolar" emission pattern has $k=2$, i.e., it represents "alignment," while the "quadrupolar" pattern is of rank $k=4$ and should be more correctly referred to as "hexadecapole." Individually, the range of the multipole parameters are $-1 \leqslant \beta \leqslant 2$, and $-1 \leqslant \gamma \leqslant 7/3$, the highest order of anisotropy $k=4$ is consistent with two-photon absorption

$$k \leqslant 2N. \tag{19}$$

Higher anisotropy coefficients beyond $k=4$ are not detectable. By projecting the numerically calculated angular distributions to Eq. (18), we obtain the β and the γ parameters listed in Table I. Near the IP ionization peaks (37 and 39 eV for 450 and 150 as pulses, respectively) β is at least one order of magnitude larger than γ. The β values are very close to their maximum value of 2. At 52 eV, near the CI valley, β and γ become comparable, giving rise to a strong mixing of dipole and quadrupole terms in the angular distributions.

It should be noted that the present deviation from a strictly aligned $(k=2)$ pattern is due to multiphoton effects and not due to retardation effects beyond the dipole approximation [29]. Figures 5 and 6 clearly show that two-photon IP ionization features a near Hertz dipole distribution while CI ionization possess a significant $k=4$ admixture. It is now instructive to relate the origin of the quadrupole component

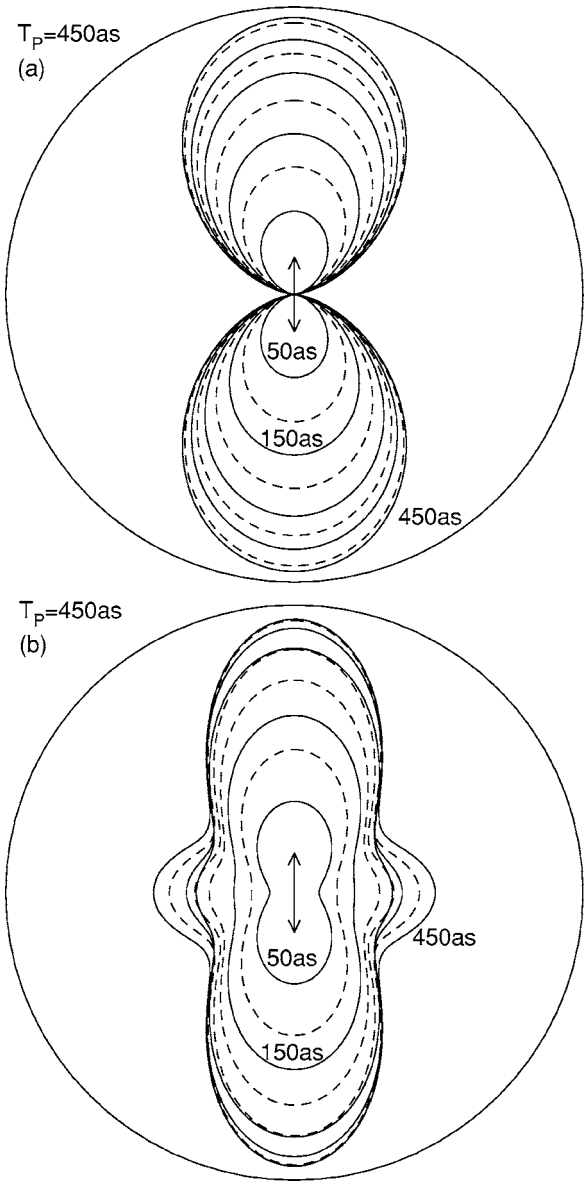

FIG. 5. The angular distribution (polar plot) of the ejected electrons for an XUV pulse with $\tau_p=450$ as. Snap shots of lines of constant intensities are taken at times 50 to 450 in steps of 50 as (from inside going outward) after the pulse's rise to half maximum, for energies 37 eV (left) and 52 eV (right). The unit circle indicates intensities of 7×10^{-6} eV^{-1} for (a) and 6×10^{-7} eV^{-1} for (b). The arrows show the polarization axis.

to correlations. A nonvanishing γ requires a final state in the continuum with $L_f=2$ since $k=2L_f$. The latter results from coupling of configurations involving single-particle orbitals $(l_f,l_f'):(s_fd_f),(p_fp_f)$, and (d_fd_f), where the latter is already negligible at the present intensity. By selectively switching off final states consisting of (s_fd_f) and (p_fp_f) configurations we find that the IP ionization peak is dominated by (p_fp_f) orbitals while the CI ionization contribution is dominated by (s_fd_f) contributions. These final states can be reached by absorption of two photons along the LOPT pathways that correspond to either diagram [Fig. 2(b)]

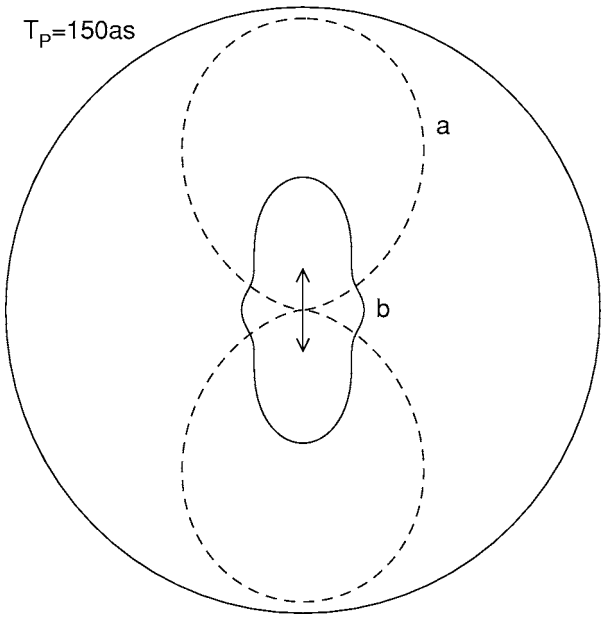

FIG. 6. Polar plots of the angular distribution of the ejected electrons after a pulse with $\tau_p=150$ as. The distribution (a) is taken at 39 eV and (b) at 52 eV. The unit circle indicates an intensity of 3×10^{-7} eV^{-1}. The arrows show the polarization axis.

$$(s_i \overset{\text{xuv}}{\rightarrow} s_f, s_i \overset{\text{xuv}}{\rightarrow} p \rightarrow d_f) \tag{20a}$$

or diagram [Fig. 2(a)]

$$(p_i \overset{\text{xuv}}{\rightarrow} s_f, p_i \overset{\text{xuv}}{\rightarrow} d_f). \tag{20b}$$

While the first path [Eq. (20a)] can be realized for the dominant configuration in the initial state (s_i,s_i) [see Eq. (5)] and would be present for an uncorrelated initial state described by, e.g., HF wave function, the second path (20b) has as prerequisite configuration admixtures (p_i,p_i) to the initial state and thus initial-state angular correlation. When selectively eliminating the (p_i,p_i) configuration from the initial state we find that the cross section in the valley region is reduced by almost an order of magnitude. This unambiguously characterizes the "anomalous" cross section component in the "valley" as being due to correlations. By contrast, the IP ionization peaks are barely affected when (p_i,p_i) configurations are removed. This is plausible as the dominant two-photon absorption process from an uncorrelated initial state according to Fig. 2(a)

TABLE I. The multipole expansion parameters β and γ Eq. (18) for the pulse durations of 450 and 150 as, at two energies each, corresponding to IP and CI ionization (see text).

τ_p	Type	Energy	β	γ
450 as	IP	37 eV	1.94	−0.08
	CI	52 eV	0.40	0.58
150 as	IP	39 eV	1.87	−0.17
	CI	52 eV	0.51	0.35

$$(s_i \xrightarrow{\text{xuv}} p_f, s_i \xrightarrow{\text{xuv}} p_f) \tag{20c}$$

predicts a dominance of a Hertz dipole pattern for each ejected electron. Our calculations suggests that initial-state correlations may be more important than final-state correlations. This is due to the fact that the pair of electrons near the symmetric energy sharing point $E_s=52$ eV leave the interaction region quickly with a relatively large speed of $v=2$ a.u.

Ishikawa *et al.* [18] have discussed the "anomalous" component in terms of two semiclassical models. Post-ionization energy exchange (PIEE) and second ionization during core relaxation (SICR). They found that PIEE is inefficient to account for the valley region consistent with our observation that final-state correlations are of minor importance. On the other hand, the relaxation process due to change in screening in the SICR appears to resemble somewhat a shake process and is as a quasi-isotropic process unlikely to yield a high-order ($k=4$) anisotropy.

V. CONCLUSIONS

We have studied the electron energy and angular distributions in two-photon double-ionization of He by an attosecond, intense soft x-ray pulse, specifically, for the Ti:sapphire 59th harmonic pulse with an intensity of 10^{15} W/cm^2. We solved the TDSE with our coupled channel method in which the electron-electron interaction is fully taken into account.

The electron energy distributions show well-localized peaks for pulse of long duration τ_p. They are understood to arise from the independent-particle (IP) ionization. For short pulses of only a few hundred attoseconds, the peaks shift toward each other and the cross section in the valley between the peaks becomes significant. We attribute this ionization component to the correlation-induced (CI) ionization. We investigated the electron angular distributions from IP and CI ionization. We find shape profiles to be that of a Hertz dipole for IP ionization but a significant admixture of a $k=4$ ("quadrupole") components for CI ionization. The unique signature of correlation-induced ionization is the presence of this $k=4$ component in the angular shape profiles. They were further quantified in terms of the multipole expansion parameters.

Time evolution of the electron angular distribution suggests that sequentiality of electron ejection or photon absorption is neither relevant nor well defined. Clearly, further studies are needed to clarify electron correlation effects. Joint energy-angular distributions (i.e., kinematically complete momentum distributions) would provide new insight into the ionization mechanism. It would also be useful to understand the ionization with the help of a perturbative approach, either with the electron-electron interaction or the pulse intensity as the expansion parameter. This would provide a complementary picture to various mechanisms that may be difficult to identify in fully numerical TDSE results.

ACKNOWLEDGMENTS

We would like to thank Dr. Ishikawa for providing us their unpublished results. This work was supported by SFB 016-FWF and EU-HITRAP, Project Number HPRI-CT-2001-50067.

[1] R. Kienberger, E. Gouliemakis, M. Uiberacker, A. Baltuska, V. Yakovlev, F. Bammer, A. Scrinzi, Th. Westerwalbesloch, U. Kleinberg, U. Heinzmann, M. Drescher, and F. Krausz, Nature (London) **427**, 817 (2004).
[2] T. Sekikawa, A. Kosuge, T. Kanai and S. Watanabe, Nature (London) **432**, 605 (2004).
[3] H. Hasegawa, E. J. Takahashi, Y. Nabekawa, K. L. Ishikawa, and K. Midorikawa, Phys. Rev. A **71**, 023407 (2005).
[4] J. Samson, Z. He, L. Yin, and G. Haddad, J. Phys. B **27**, 887 (1994).
[5] J. C. Levin, G. B. Armen, and I. A. Sellin, Phys. Rev. Lett. **76**, 1220 (1996).
[6] R. Dörner *et al.*, Phys. Rev. Lett. **76**, 2654 (1996).
[7] K. W. Meyer, C. H. Greene, and B. D. Esay, Phys. Rev. Lett. **78**, 4902 (1997).
[8] Y. Qiu, J. Tang, J. Burgdörfer, and J. Wang, Phys. Rev. A **57**, R1489 (1998).
[9] L. Spielberger *et al.*, Phys. Rev. Lett. **74**, 4615 (1995); L. Spielberger *et al.*, Phys. Rev. A **59**, 371 (1999).
[10] L. Andersson and J. Burgdörfer, Phys. Rev. A **50**, R2810 (1994); T. Suric, K. Pisk, B. A. Logan, and R. H. Pratt, Phys. Rev. Lett. **73**, 790 (1994).
[11] L. Feng and H. V. van der Hart, J. Phys. B **36**, L1 (2003).
[12] S. Laulan and H. Bachau, Phys. Rev. A **68**, 013409 (2003).
[13] S. Laulan and H. Bachau, Phys. Rev. A **69**, 033408 (2004).
[14] J. Colgan and M. S. Pindzola, Phys. Rev. Lett. **88**, 173002 (2002).
[15] P. Lambropoulos, L. A. A. Nikolopoulos, and M. G. Makris, Phys. Rev. A **72**, 013410 (2005).
[16] B. Walker *et al.*, Phys. Rev. Lett. **73**, 1227 (1994).
[17] J. S. Parker, R. L. Moore, K. J. Meharg, D. Dundas, and K. T. Taylor, J. Phys. B **34**, L69 (2001).
[18] K. L. Ishikawa and K. Midorikawa (private communication); Phys. Rev. A **72**, 013407 (2005).
[19] I. F. Barna, Ph.D. thesis, University Giessen, Giessen, 2002, http://geb.uni-giessen.de/geb/volltexte/2003/1036
[20] I. F. Barna, N. Grün, and W. Scheid, Eur. Phys. J. D **25**, 239 (2003).
[21] I. F. Barna, K. Tőkési, and J. Burgdörfer, J. Phys. B **38**, 1001 (2005).
[22] I. F. Barna and J. M. Rost, Eur. Phys. J. D **27**, 287 (2003); I. F. Barna, *ibid.* **33**, 307 (2005).
[23] E. J. Takahashi, Y. Nabekawa, and K. Midorikawa, Appl. Phys. Lett. **84**, 4 (2004).
[24] J. H. McGuire, *Electron Correlation Dynamics in Atomic Collisions* (Cambridge University Press, Cambridge, 1997).
[25] P. B. Corkum, Phys. Rev. Lett. **71**, 1994 (1993).
[26] T. Weber *et al.*, Nature (London) **405**, 658 (2000); R. Moshammer *et al.*, Phys. Rev. Lett. **84**, 447 (2000).
[27] F. Lindner *et al.*, Phys. Rev. Lett. **95**, 040401 (2005).
[28] F. Byron and C. Joachain, Phys. Rev. **164**, 1 (1967).
[29] A. Derevianko *et al.*, Phys. Rev. Lett. **84**, 2116 (2000).